*J. Fluid Mech.* (1988), *vol.* 189, *pp.* 311–335
*Printed in Great Britain*



# Particle size segregation in inclined chute flow of dry cohesionless granular solids

By S. B. SAVAGE AND C. K. K. LUN
Department of Civil Engineering and Applied Mechanics, McGill University, Montreal, Canada H3A 2K6

(Received 1 September 1986 and in revised form 19 November 1987)

If granular materials comprising particles of identical material but different sizes are sheared in the presence of a gravitational field, the particles are segregated according to size. The small particles fall to the bottom and the larger ones drift to the top of the sheared layer. In an attempt to isolate and study some of the essential segregation mechanisms, the paper considers a simplified problem involving the steady two-dimensional flow of a binary mixture of small and large spherical particles flowing down a roughened inclined chute. The flow is assumed to take place in layers that are in motion relative to one another as a result of the mean shear. For relatively slow flows, it is proposed that there are two main mechanisms responsible for the transfer of particles between layers. The first mechanism, termed the 'random fluctuating sieve', is a gravity-induced, size-dependent, void-filling mechanism. The probability of capture of a particle in one layer by a randomly generated void space in the underlying layer is calculated as a function of the relative motion of the two layers. The second, termed the 'squeeze expulsion' mechanism, is due to imbalances in contact forces on an individual particle which squeeze it out of its own layer into an adjacent one. It is assumed that this mechanism is not size preferential and that there is no inherent preferential direction for the layer transfer. This second physical mechanism in particular was proposed on the basis of observations of video recordings that were played back at slow speed. Since the magnitude of its contribution is determined by the satisfaction of overall mass conservation, the exact physical nature of the mechanism is of less importance. By combining these two proposed mechanisms the net percolation velocity of each species is obtained. The mass conservation equation for fines is solved by the method of characteristics to obtain the development of concentration profiles with downstream distance. Although the theory involves a number of empirical constants, their magnitude can be estimated with a fair degree of accuracy. A solution for the limiting case of dilute concentration of fine particles and a more general solution for arbitrary concentrations are presented. The analyses are compared with experiments which measured the development of concentration profiles during the flow of a binary mixture of coarse and fine particles down a roughened inclined chute. Reasonable agreement is found between the measured and predicted concentration profiles and the distance required for the complete separation of fine from coarse particles.

## 1. Introduction

When a randomly mixed mass of granular material consisting of particles of different sizes and densities is sheared in the presence of a gravitational field, segregation or grading of the particles over the flow depth usually occurs. The coarse

low-density particles drift towards the top of the sheared layer; these are followed somewhat lower down by the fine low-density and coarse high-density particles, with the fine dense particles collecting on the bottom. This phenomenon is evident to anyone who, having purchased a box of popcorn at the cinema, notices how the small unpopped corn kernels end up at the bottom of the container. Devices such as pinched sluices, Humphreys spirals and Reichert cones are widely used in mineral processing (Wills 1979) for sorting materials of different sizes, materials of different densities, concentrates from tailings, etc. Such devices take advantage of the mechanism of gravity separation when granular materials in the form of slurries or in the dry state are made to flow down inclined surfaces. There seems to be little detailed understanding of, or consensus about, the mechanics of how these devices operate despite the fact that pinched sluices have been used for centuries and despite the fact that they, their more modern counterpart the Reichert cone, and spiral concentrators such as the Humphreys spiral are installed in large numbers of plants throughout the world. On the other hand, there are instances arising during the manufacture of pharmaceuticals, detergents, animal feeds, fertilizers, plastics, ceramics, etc. where the goal is to uniformly mix two or more particulate solids. Gravity separation can be a source of frustration in systems involving cohesionless particles of different sizes (Bridgwater 1976). If the mixing device is operated for too long a time, mixture quality deteriorates and demixing occurs after an initial period of favourable mixing.

A phenomenon related to the above gravity separation mechanism is observed in connection with deposition of sediments in a geological context; it is known as 'reverse' or 'inverse' grading (Middleton 1970; Middleton & Hampton 1976; Naylor 1980; Sallenger 1979; Walker 1973). This is in contrast to 'normal grading' in which the finer particles are found in the upper layers of a lake or river bed and the coarse ones are lower down. In normal grading when a mass of particles is discharged into the water, the faster-falling large particles reach the bed first and the slowest-falling fine particles are deposited last and form the top of the bed. Reverse grading in which the sizes occur in reverse order is believed to result from grain flows (Bagnold 1954) analogous to sand avalanching in which dispersions of cohesionless sediments move down inclines under the action of gravity.

Investigations into the mechanics of percolation and segregation of dry granular materials are of fairly recent origin. Our present understanding owes much to the numerous fundamental theoretical and experimental studies of Bridgwater and his co-workers (Bridgwater 1971; Campbell & Bridgwater 1973; Masliyah & Bridgwater 1974; Scott & Bridgwater 1975; Bridgwater 1976; Bridgwater, Cooke & Scott 1978; Cooke, Bridgwater & Scott 1978; Cooke & Bridgwater 1979; Drahun & Bridgwater 1981, 1983; Foo & Bridgwater 1983; Bridgwater, Cook & Drahun 1985*a*; Bridgwater, Foo & Stephens 1985*b*, etc.).

Drahun & Bridgwater (1983) have studied free-surface segregation which occurs when particles are poured on to a heap. The effects of particle size, density and shape, free-fall height on to the heap, the manner of feeding of particles, etc. were studied. While this work is related in some ways to the present study, the flow that develops is a very complicated one. Several different segregation mechanisms are at work. The flow can be unsteady with periodic avalanching of particles as material builds up beneath the pouring point.

Bridgwater *et al.* (1985*b*) used a continuum approach to investigate the development over time of particle mixing and segregation in a failure zone of an annular shear cell. It was assumed that the diffusive flux was linearly dependent

upon concentration gradient with the diffusive coefficient being dependent upon both strain rate and mixture coefficient. The evolution of the concentration profiles in the failure zone was obtained by the method of characteristics.

Walton (1983) has performed computer simulations of two-dimensional flows of circular and polygonal shaped disk-like particles flowing down inclined chutes. Segregation of different sized particles was observed in these simulations but the rates were lower than those observed in the experiments to be described in the present paper. One would expect that segregation rates in these simulations would be less than those in a real physical situation because of geometric restrictions. For flow down a given slope the occurrence of void spaces of sufficient size to permit transfer of particles from one layer to another is less likely in two than in three dimensions.

The present paper describes an investigation of the mechanics of the size segregation process during the relatively slow flow of dry particles of equal mass density down a roughened inclined chute. We consider the case in which a binary mixture of small and large spherical particles enters the upstream end of the chute. It is assumed that the chute is inclined such that the particles flow at constant depth with constant streamwise velocity profiles. The concentration of small particles is taken to be uniform over the depth at the entry and we investigate the size segregation process as the flow proceeds downstream. By making use of information-entropy concepts and extending the approach of Cooke & Bridgwater (1979), the net percolation velocities of the small and large particles are obtained. The mass conservation equation for the small particles is solved by the method of characteristics for the limiting case of dilute concentrations to obtain the development of the concentration profiles with downstream distance. A similar but more general analysis for arbitrary concentrations is also presented. Experiments were performed using a binary mixture of spherical polystyrene beads flowing down a roughened inclined chute. Concentration profiles measured at various distances downstream of the flow entry are compared with predictions of both the dilute and general theories.

## 2. Proposed physical mechanisms

We shall attempt to isolate and study some of the essential segregation mechanisms by considering a simplified problem involving the steady two-dimensional flow of a binary mixture of small and large spherical particles of equal mass density down a roughened inclined chute. We assume that the flow takes place in layers which are in motion relative to one another as a result of the mean shear developed by the rough lower boundary (figure 1).

For flows that are not too fast and in which the particle velocity fluctuations arising from collisions are not too vigorous, it is proposed that there are two main mechanisms responsible for the transfer of particles between layers. Our proposal is based upon visual observations of video tapes made during the experiments described in §7. The tapes were played back at slow speed and the motion of individual grains in the region of the transparent glass sidewalls could be observed. Because of overriding of layers and the continual rearrangement of particles within a layer, the contact force network and the void spaces are undergoing continual random changes. At any instant, there will be a distribution of void spaces in a given layer. If a void space is large enough, then a particle from the layer above can fall into it as the layers move relative to one another. For a given overall solids concentration, the probability of finding a hole that a small particle can fall into is

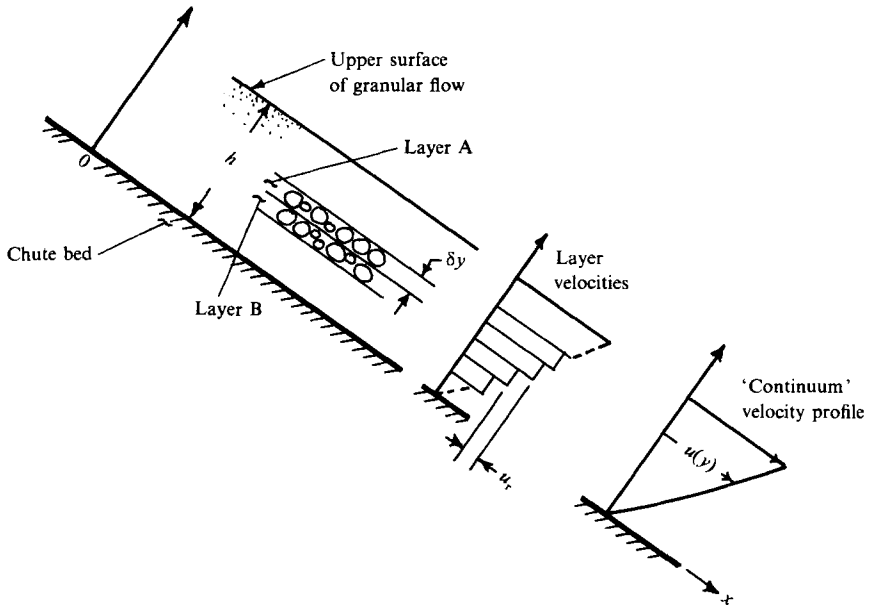


FIGURE 1. Flow of particles in layers down a rough inclined chute.

larger than the probability of finding a hole that a large particle can fall into. Hence, there is a tendency for particles to segregate out, with fines at the bottom and coarse ones at the top. This gravity-induced size-dependent void filling mechanism we term the 'random fluctuating sieve' mechanism. Our second proposed mechanism is less apparent but was suggested by the slow-motion videotapes of the segregation process. If the instantaneous forces acting on an individual particle are sufficiently imbalanced, the particle can be squeezed out of its own layer into an adjacent one. We assume that this mechanism, which we term 'squeeze expulsion', is not size preferential and that there is no inherent preferential direction for the layer transfer. It is important to note that the correctness of details of the physical explanation of this second mechanism is not essential. One just requires some additional means to satisfy the condition that there is no overall mass flux in the direction normal to the plane of the inclined chute.

We have proposed only two main mechanisms for the transfer or migration of particles across the shear layer. Although we believe these are the two most important ones for the slow, dense shearing flows of present interest, it should be noted that in more general flows several other mechanism exist, as has been discussed by Williams (1976), Johanson (1978) and Drahun & Bridgwater (1983). The ideas discussed above will now be developed in a more quantitative form.

## 3. Random fluctuating sieve model

### 3.1. *Distribution of voids in a layer*

During the shearing process in the proposed model it is necessary to decide whether a particle from the upper layer can fall into a hole in the underlying layer. To do so requires information about the likely distribution of the sizes of the void spaces in some region of the underlying layer. A simple and convenient way to determine this distribution function is by means of the 'maximum-entropy approach' (Jaynes 1963; Brown 1978) as follows.

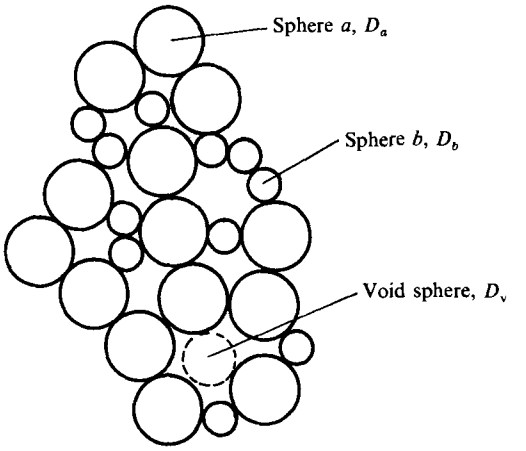


FIGURE 2. 'Random continuous network' for binary mixture of small and large spherical particles in a layer.

Consider a binary mixture of spherical particles of equal mass density in a 'region' or 'neighbourhood' in one layer. The large and small particles are of diameters $D_a$ and $D_b$ respectively. We assume that the particles at any instant make up a 'random continuous' network (see Zallen 1983, pp. 60–71) as shown in figure 2. Define a 'void sphere' of diameter $D_v$ as the largest sphere that can fit into a given void space formed by the random continuous network. We discretize such that each void sphere is associated with one of $m$ states corresponding to a particular void sphere diameter $D_{v_i}$. Now define a void diameter ratio

$$E_i = \frac{D_{v_i}}{\bar{D}}, \tag{3.1}$$

where

$$\bar{D} = \frac{n_a D_a + n_b D_b}{n_a + n_b} \tag{3.2}$$

is the mean particle diameter in a neighbourhood, and $n_a$ and $n_b$ are the number of large and small particles in that neighbourhood. Thus

$$E_i = \frac{D_{v_1}(1+\eta)}{D_a(1+\eta\sigma)}, \tag{3.3}$$

where

$$\eta = n_b/n_a, \tag{3.4}$$

$$\sigma = D_b/D_a. \tag{3.5}$$

Let $M_i$ equal the number of void spheres to which the $i$th state (corresponding to a particular void diameter ratio $E_i$) is assigned, then

$$\sum_{i=1}^{m} M_i = M \tag{3.6}$$

is the total number of voids in the neighbourhood. Any distribution $M_i$ corresponds to a specific *microstate*. The number of ways to realize a specific microstate, or in other words the number of ways to distribute $M$ void spaces over $m$ states is

$$W = \frac{M!}{M_1! M_2! \ldots M_m!}. \tag{3.7}$$

Making use of Stirling's approximation we find

$$\log W = -M \sum_{i=1}^{m} \frac{M_i}{M} \log\left(\frac{M_i}{M}\right), \tag{3.8}$$

where $\log W$ corresponds to the information entropy (Jaynes 1963; Brown 1978).

The probability of finding a voids sphere corresponding to the $i$th state is given by

$$p_i = \frac{M_i}{M} \tag{3.9}$$

and

$$\sum_{i=1}^{m} p_i = \sum_{i=1}^{m} \frac{M_i}{M} = 1. \tag{3.10}$$

Also, we have

$$\sum_{i=1}^{m} p_i E_i = \bar{E} = \frac{\bar{D}_v}{\bar{D}}, \tag{3.11}$$

where $\bar{E}$ is the mean void diameter ratio defined as the ratio of the mean void diameter $\bar{D}_v$ to $\bar{D}$, the mean particle diameter of the neighbourhood.

If all states are equally probable, then the most probable way of assignment is the one that maximizes (3.8) subject to the constraints (3.10) and (3.11). We thus find the probability of finding a voids diameter ratio $E = D_v/\bar{D}$ as

$$p(E) = \frac{1}{\bar{E}-E_m} \exp\left\{-\frac{E-E_m}{\bar{E}-E_m}\right\}, \tag{3.12}$$

where $E_m$ is the minimum possible voids diameter ratio. For the closest packing of equal spheres $E_m = 0.1547$.

Now define a voids area ratio in a neighbourhood as the ratio of the total projected area of the voids to the projected area of the solids, i.e.

$$e_A = \frac{M\bar{A}_{v_T}}{n_a A_a + n_b A_b}, \tag{3.13}$$

where $M$ is the total number of voids in the neighbourhood, $\bar{A}_{v_T}$ is the mean projected total voids area, $A_a = \frac{1}{4}\pi D_a^2$ and $A_b = \frac{1}{4}\pi D_b^2$ are the projected areas of the large and small spheres respectively. Define $k_{AV}$ as the ratio of the mean voids sphere projected area to the mean projected total voids area $\bar{A}_{v_T}$,

$$k_{AV} = \frac{\bar{A}_{v_s}}{\bar{A}_{v_T}}, \tag{3.14}$$

where the mean voids sphere projected area

$$\bar{A}_{v_s} = \tfrac{1}{4}\pi \bar{D}_v^2. \tag{3.15}$$

The total number of particles in the region

$$N = n_a + n_b. \tag{3.16}$$

Since

$$\bar{E} = \frac{\bar{D}_v(1+\eta)}{D_a(1+\eta\sigma)}$$

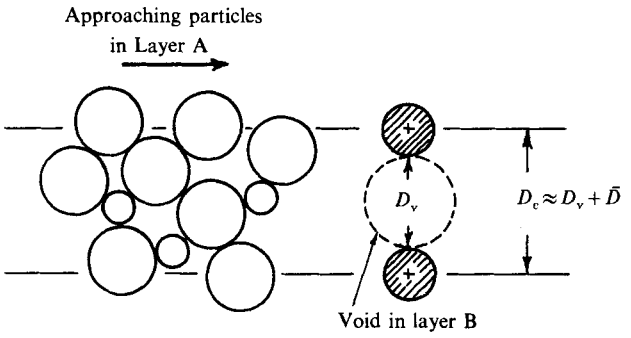


FIGURE 3. Capture of particles by void in lower layer B.

we can rewrite (3.13) using (3.14), (3.15) and (3.16) as

$$e_A = \frac{M}{N}\frac{\bar{E}^2}{k_{\mathrm{AV}}}\frac{(1+\eta\sigma)^2}{(1+\eta)(1+\eta\sigma^2)}, \tag{3.17}$$

where $M/N$ is the ratio of the number of voids to the number of particles in a layer neighbourhood. For example, for a cubic packing of equal particles $M/N = 1$; for closest packing of equal particles, $M/N = 2$; for a regular hexagonal array around a void of equal diameter, $M/N = 0.5$; etc. For a random continuous network, we assume that we can choose values for $M/N$ and $k_{\mathrm{AV}}$ appropriate for the mean voids diameter ratio associated with the neighbourhood.

### 3.2. *'Capture' of a particle*

We now consider how a particle from layer A (see figure 1) is captured by a void space in the underlying layer B. Figure 3 shows a void with void diameter $D_v$ and two adjacent (cross-hatched) spheres all in the layer B. A particle from the upper layer A will be directed towards the void if its centre lies within the capture region defined by the capture diameter $D_c$ equal to the sum of the void diameter $D_v$ and the radii of the two adjacent cross-hatched spheres in layer B. We take $D_c$ to be given approximately by

$$D_c \approx D_v + \bar{D} = \bar{D}(E+1). \tag{3.18}$$

We define the number of particles per unit area in a layer as

$$\begin{aligned} n_p &= \frac{n_a + n_b}{(1+e_A)(n_a A_a + n_b A_b)} \\ &= \frac{(1+\eta)}{A_a(1+e_A)(1+\eta\sigma^2)} \end{aligned} \tag{3.19}$$

The number of voids per unit area in a region is defined as

$$n_v = n_p(M/N) \tag{3.20}$$

The number of particles 'captured' by a void per unit time is $u_r D_c n_p$, where $u_r$ is the mean downstream velocity of the particles in a layer *relative* to those in the underlying layer. The number of small, $b$, particles captured by a void per unit time is

$$\frac{n_b}{n_a + n_b} u_r D_c n_p.$$

The number of $b$ particles captured per unit area per unit time by voids having diameters between $D_v$ and $D_v + dD_v$ is

$$n_v \frac{n_b}{n_a + n_b} u_r D_c n_p p \, dE.$$

The $b$ particles drop from layer A into the void in the underlying layer B if the void space is large enough, i.e. if $E > D_b/\bar{D} = E_b$. Hence, the number of small, $b$, particles per unit area per unit time that fall into the voids (i.e. towards the bed) is

$$N_b = \int_{E_b}^{\infty} n_v \frac{n_b}{n_a + n_b} u_r \bar{D}(E+1) n_p p \, dE, \tag{3.21}$$

and using (10)

$$N_b = n_v \frac{n_b}{n_a + n_b} n_p u_r \bar{D}[E_b + \bar{E} - E_m + 1] \exp\left\{-\frac{E_b - E_m}{\bar{E} - E_m}\right\}. \tag{3.22}$$

Similarly the number of large, $a$, particles per unit area per unit time that fall into voids is

$$N_a = n_v \frac{n_a}{n_a + n_b} n_p u_r \bar{D}[E_a + \bar{E} - E_m + 1] \exp\left\{-\frac{E_a - E_m}{\bar{E} - E_m}\right\}, \tag{3.23}$$

where $E_a = D_a/\bar{D}$.

### 3.3. *Continuum quantities*

We now define continuum or averaged percolation velocities and densities for the small and large sphere components. Thus, we write the mass flux of the small, $b$, particles in the direction normal to the incline as

$$\rho_b q_b = -m_b N_b, \tag{3.24}$$

where $m_b$ is the mass of an individual $b$ particle, $q_b$ is the 'continuum' or volume-averaged velocity of the $b$ particles in the positive $y$-direction (see figure 1) and $\rho_b$ is the mass of components $b$ per unit volume, which can be expressed as

$$\rho_b = \frac{\rho_s \eta \sigma^3}{(1+e)(1+\eta\sigma^3)}, \tag{3.25}$$

where $e$ is the *volume* voids ratio (i.e. the volume of voids/volume solids) and $\rho_s$ is the solid material mass density. Similarly for the large, $a$, component we find

$$\rho_a q_a = -m_a N_a, \tag{3.26}$$

where the mass of component $a$ per unit volume is

$$\rho_a = \frac{\rho_s}{(1+e)(1+\eta\sigma^3)}. \tag{3.27}$$

The bulk density of the mixture is given by

$$\rho = \rho_a + \rho_b = \frac{\rho_s}{1+e} = \rho_s \nu, \tag{3.28}$$

where $\nu$ is the solids volume fraction (i.e. the volume of solids per unit volume).

The relative velocity between layers, $u_r$, may be written as

$$u_r = \frac{du}{dy}\delta y, \tag{3.29}$$

where $u$ is the continuum or bulk velocity in the $x$-direction (figure 1) and $\delta y$ is the particle-layer thickness which we approximate as

$$\delta y = k_{LT}\bar{D}, \tag{3.30}$$

and $k_{LT}$ is a layer-thickness constant and is close to unity. Now

$$\nu = \frac{1}{1+e} = n_p\left[\frac{n_a V_a + n_b V_b}{n_a + n_b}\right]/k_{LT}\bar{D}, \tag{3.31}$$

where $V_a = \frac{1}{6}\pi D_a^3$ and $V_b = \frac{1}{6}\pi D_b^3$ are the volumes of the large and small spheres respectively. Using (3.2) and (3.19) we may express (3.31) as

$$\nu = \frac{2(1+\eta)(1+\eta\sigma^3)}{3k_{LT}(1+e_A)(1+\eta\sigma^2)(1+\eta\sigma)}. \tag{3.32}$$

## 4. Squeeze expulsion and net percolation velocities

Both of the percolation velocities $q_a$ and $q_b$ that we have just calculated turn out to be negative, i.e. towards the rigid impermeable bed. Thus, there must be another mechanism for transfer of particles from one layer to another which gives rise to a counterflow so as to yield a zero net mass flux in the $y$-direction. (Note that we have assumed the flow depth, velocity profiles and overall solids fraction to be independent of streamwise distance.) It is proposed that, as a result of the fluctuating contact forces on an individual particle, there can occur force imbalances such that a particle is 'squeezed' out of its own layer into an adjacent one if an opening is available or the force imbalance is sufficiently large. This mechanism is not gravity driven and it is supposed that it is not size preferential. Thus, setting the mass flux in the $y$-direction to zero, we obtain

$$\rho_a q_a + \rho_b q_b + \rho q_{SE} = 0, \tag{4.1}$$

where $\rho$ is the bulk density given by (3.28) and $q_{SE}$ is the continuum or bulk squeeze-expulsion velocity for the mixture. We can rewrite (4.1) as

$$\rho_a q_{a_{NET}} = -\rho_b q_{b_{NET}}, \tag{4.2}$$

where

$$q_{a_{NET}} = q_a + q_{SE}, \quad q_{b_{NET}} = q_b + q_{SE} \tag{4.3}$$

are the *net* volume-averaged percolation velocities of the $a$ and $b$ components respectively.

The velocity $q_{SE}$ has been named the squeeze-expulsion velocity because this mechanism seems to us from our visual observations of video-tapes of the segregation process to be the main one responsible for the counterflow. However, $q_{SE}$ is necessary to satisfy overall mass conservation (4.1) and it could be due to a number of different mechanisms.

The net mass fluxes in the $y$-direction may be written using (3.24), (3.26), (4.1) and (4.3) as

$$\rho_a q_{a_{\mathrm{NET}}} = \frac{\rho_a \rho_b}{\rho}(q_a - q_b) = -\frac{\rho_b}{\rho} m_a N_a + \frac{\rho_a}{\rho} m_b N_b, \tag{4.4a}$$

$$\rho_b q_{b_{\mathrm{NET}}} = \frac{\rho_a \rho_b}{\rho}(q_b - q_a) = \frac{\rho_b}{\rho} m_a N_a - \frac{\rho_a}{\rho} m_b N_b. \tag{4.4b}$$

Note that the particles are also translated in the $x$-direction with the mean transport velocity $u(y)$. Thus, the volume-averaged velocity vectors for the $a$ and $b$ components are

$$\boldsymbol{v}_a = u(y)\,\boldsymbol{i} + q_{a_{\mathrm{NET}}}\boldsymbol{j}, \quad \boldsymbol{v}_b = u(y)\,\boldsymbol{i} + q_{b_{\mathrm{NET}}}\boldsymbol{j}, \tag{4.5}$$

and the bulk velocity of the mixture is

$$\boldsymbol{v} = \frac{\rho_a}{\rho}\boldsymbol{v}_a + \frac{\rho_b}{\rho}\boldsymbol{v}_b. \tag{4.6}$$

### 4.1. *Net percolation velocity for dilute case, $\eta \to 0$*

We define the volume concentration of small, $b$, particles in a neighbourhood as the ratio of the local volume of the $b$ particles to the total volume of particles in the mixture in that neighbourhood. Thus

$$C_b = \frac{\eta\sigma^3}{1+\eta\sigma^3}. \tag{4.7}$$

Consider the case of a dilute concentration of small particles in which the number density ratio $\eta \to 0$.

Now using (3.2), (3.17), (3.19), (3.22), (3.23), (3.25) and (3.27) in (4.4) and retaining the leading terms for $\eta \to 0$ we obtain the following expression for the non-dimensional net percolation velocity for the $b$ particles:

$$\tilde{q}_{b_{\mathrm{NET}}} = \frac{-q_{b_{\mathrm{NET}}}}{D_a(\mathrm{d}u/\mathrm{d}y)} = -\frac{4}{\pi}\frac{M}{N}\frac{k_{\mathrm{LT}}^2}{[1+(\bar{E}^2/k_{\mathrm{AV}})(M/N)]}\left[(2+\bar{E}-E_{\mathrm{m}})\exp\left[-\frac{1-E_{\mathrm{m}}}{\bar{E}-E_{\mathrm{m}}}\right]\right.$$
$$\left. -(\sigma+\bar{E}-E_{\mathrm{m}}+1)\exp\left[-\frac{\sigma-E_{\mathrm{m}}}{\bar{E}-E_{\mathrm{m}}}\right]\right]. \tag{4.8}$$

Cooke & Bridgwater (1979) and Bridgwater *et al.* (1978) have reported percolation velocities measured during experiments in which a single small particle (or in some cases a small number of particles) fell through a sheared bed of larger particles. The larger particles were contained in a shear box having two vertical sidewalls and two sidewalls that could rotate about hinges at the base, deforming the rectangular box into a parallelogram in reciprocating fashion. In earlier versions of the shear box the strain rate varied sinusoidally with time, but in later versions the strain rate was constant during the time between reversals. The results of these later tests are suitable for comparison with the predictions of (4.8).

In order to determine values of the net percolation velocity $q_{b_{\mathrm{NET}}}$ from (4.8) we need value for $M/N$, $\bar{E}$, $k_{\mathrm{AV}}$ and $k_{\mathrm{LT}}$. We can easily calculate $M/N$, $\bar{E}$, and $k_{\mathrm{AV}}$ for various packings of equal-sized particles around a void. Some values are listed in table 1.

A rough and simple way to obtain a consistent set of values $M/N$, $E$, and $k_{\mathrm{AV}}$ is to plot the values in table 1 versus the number of particles around a void in a layer,

| Number of particles around void in a layer | $M/N$ | $\bar{E}$ | $k_{AV}$ |
|---|---|---|---|
| 3 (closest packing) | 2 | 0.1547 | 0.466 |
| 4 (simple cubic) | 1 | 0.414 | 0.63 |
| 5 | 0.6 | 0.701 | 0.712 |
| 6 | 0.5 | 1 | 0.765 |

TABLE 1

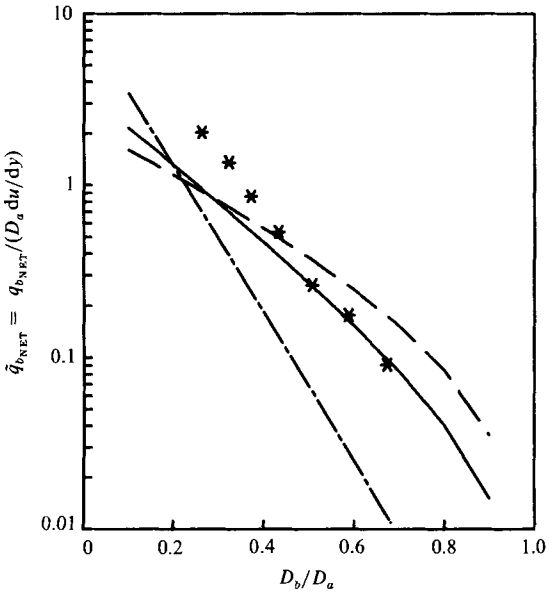


FIGURE 4. Comparison of predicted net percolation velocity versus particle diameter ratio with experimental results of Bridgwater *et al.* (1978) and Cooke & Bridgwater (1979) (*). Lines represent equation (4.8) from present dilute theory using: ——, $M/N = 1.0$, $\bar{E} = 0.414$, $k_{AV} = 0.63$ and $\nu = 0.524$; – – –, $M/N = 1.2$, $\bar{E} = 0.33$, $k_{AV} = 0.59$ and $\nu = 0.546$; —·—, $M/N = 1.48$, $\bar{E} = 0.25$, $k_{AV} = 0.55$ and $\nu = 0.571$.

make a reasonable estimate of the number of particles around a void for the case of interest and interpolate for the corresponding values of $M/N$, $\bar{E}$ and $k_{AV}$. Making use of these values in (3.17) and (3.32), taking $k_{LT} = 1.0$ and letting $\eta \to 0$ gives the corresponding values for $\nu$.

Figure 4 shows the predicted values of the non-dimensional net percolation velocity $q_{v_{NET}}/(D_a\,du/dy)$ versus the ratio of particle diameters $\sigma$ compared with the experimental measurements of Bridgwater *et al.* (1978). Calculations are shown for values of $\nu$ equal to 0.524, 0.546 and 0.571. A value of $\nu = 0.546$ seems to be reasonable for a mass of spherical particles undergoing cyclical shear as in the experimental apparatus. For this value of $\nu$ and for diameter ratios $\sigma \gtrsim 0.5$, the predicted percolation velocities are close to the experimental values but the predictions are too low for $\sigma < 0.5$, the discrepancy increasing with decreasing $\sigma$. Note that for $\sigma < 0.1547$ spontaneous percolation would occur, i.e. small particles could percolate through the matrix of larger particles simply as a result of gravity,

even in the absence of any shear. The present theory is based upon the presence of shearing motion and does not account for spontaneous percolation effects. As a result, it would be expected to underpredict the percolation velocity for small $\sigma$.

## 5. Method-of-characteristics solution for dilute case, $\eta \to 0$

For a steady flow, the overall mass conservative equation is

$$\nabla \cdot (\rho \boldsymbol{v}) = 0, \tag{5.1}$$

and for each of the components

$$\nabla \cdot (\rho_a \boldsymbol{v}_a) = 0, \quad \nabla \cdot (\rho_b \boldsymbol{v}_b) = 0. \tag{5.2}$$

Substituting (4.5) into (5.2) yields for the fully developed flow ($u = u(y)$) that is under consideration here

$$u(y)\frac{\partial \rho_a}{\partial x} + \frac{\partial}{\partial y}[\rho_a q_{a_{\mathrm{NET}}}] = 0 \tag{5.3}$$

and

$$u(y)\frac{\partial \rho_b}{\partial x} + \frac{\partial}{\partial y}[\rho_b q_{b_{\mathrm{NET}}}] = 0. \tag{5.4}$$

If the velocity field $u(y)$ is known, and the distribution of concentration $G_b$ or number-density ratio $\eta$ over the depth is specified at some upstream station, say $x = 0$, then the mass conservation equation (5.2) can be solved by the method of characteristics to determine the size segregation process as the flow proceeds downstream from $x = 0$. First, we shall consider the dilute case in which $\eta \to 0$. The analysis is greatly simplified in this limit and the qualitative results are the same as in the more general case to be discussed in the next section.

From experiments on fully developed flow of particulate solids down rough inclined chutes, it has been found (see review paper of Savage 1984) that the velocity increases in a roughly linearly manner with distance from the rough bed. Thus, for the present simple analysis we approximate

$$u(y) = \gamma y, \tag{5.5}$$

where $\gamma$ is the constant shear rate.

Making the assumption that the solids volume fraction $\nu$ is constant, substituting (3.25), (4.8) and (5.5) in (5.4) and considering the dilute case where the layer number-density ratio $\eta \to 0$ we obtain

$$y\frac{\partial \eta}{\partial x} - D_a \tilde{q}_{b_{\mathrm{NET}}}\frac{\partial \eta}{\partial y} = 0. \tag{5.6}$$

The solution of (5.6) is straightforward; from the method of characteristics we find

$$\eta = \frac{n_b}{n_a} = f\left(x + \frac{y^2}{2D_a \tilde{q}_{b_{\mathrm{NET}}}}\right). \tag{5.7}$$

Thus $\eta$ is constant on the surfaces

$$y = [y_0^2 - 2D_a \tilde{q}_{b_{\mathrm{NET}}} x]^{\frac{1}{2}}, \tag{5.8}$$

where $y_0$ is a constant corresponding to the $y$-value of the characteristic line at the initial station $x = 0$. Given the distribution of $\eta$ with depth at $x = 0$, it is possible to determine the solution for $\eta$ in the downstream region. Note that had we assumed a

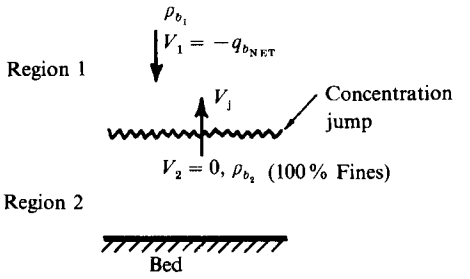


FIGURE 5. Conditions across concentration jump near bed.

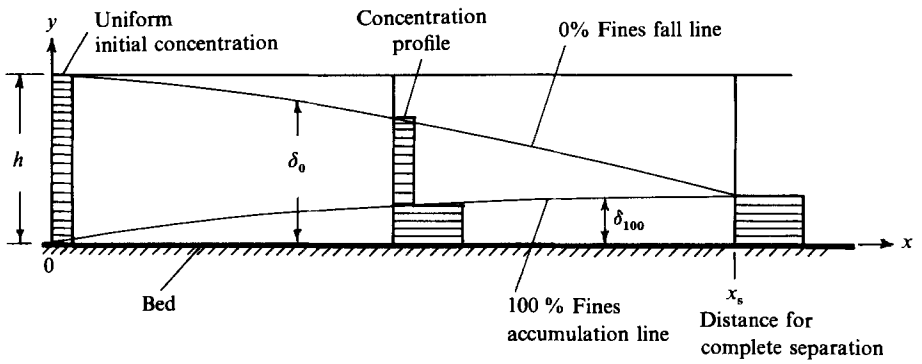


FIGURE 6. Development of concentration profiles with downstream distance.

more general velocity distribution, say a power law instead of the linear velocity profile of (5.5), the solution for $\eta$ could be obtained in a similar but still straightforward way. It would be of interest in a future investigation to examine the effects of the velocity profile on the segregation process.

The fine particles have a net percolation velocity that is towards the bed. However, since the bed is impermeable, fines must accumulate there. The amount that accumulates near the bed increases with downstream distance. Thus, a '100% fines accumulation surface' develops near the bed. This jump in concentration is analogous to a shock wave in compressible fluid flow. The characteristics solution given by (5.7) and (5.8) is valid in the region above the concentration jump.

We can determine the concentration jump velocity $V_j$ by applying conservation of mass for the $b$ particles across the jump (see figure 5). Thus, assuming the jump to be approximately parallel to the bed, we obtain

$$\rho_{b_1}(-q_{b_{NET}} + V_j) = \rho_{b_2} V_j, \tag{5.9}$$

where $\rho_{b_1}$ and $\rho_{b_2}$ are the mass densities of $b$ particles in regions 1 and 2 either side of the concentration jump. For small $\eta$, (5.9) can be written after using (3.25) and (4.8) as

$$V_j = \tilde{q}_{b_{NET}} D_a \frac{du}{dy} \eta \sigma^3. \tag{5.10}$$

We can also determine the development of the concentration shock surface by proceeding in a somewhat different way. Consider a flow of uniform depth $h$ in which the initial concentration at $x = 0$ is uniform over the depth such that

$$\eta(0, y) = \eta_0 = \text{const.} \tag{5.11}$$

The 0% fines fall line $y = \delta_0(x)$ (see figure 6) is given by (5.8) as

$$\delta_0 = [h^2 - 2D_a \tilde{q}_{b_{\mathrm{NET}}} x]^{\frac{1}{2}}. \tag{5.12}$$

We seek the 100% fines accumulation line, $y = \delta_{100}(x)$. Applying the depth-averaged conservation-of-mass equation for the fine $b$ particles yields

$$\left[\int_0^h \rho_b u \, \mathrm{d}y\right]_{x=0} = \int_0^h \rho_b u \, \mathrm{d}y = \int_0^{\delta_{100}} \rho_b u \, \mathrm{d}y + \int_{\delta_{100}}^{\delta_0} \rho_b u \, \mathrm{d}y$$
$$= \text{const.} \tag{5.13}$$

Assuming that the solids volume fraction $\nu$ is constant, substituting (3.25) and (5.7) in (5.13) yields, after some manipulation, the expression for the depth of the concentration jump

$$\delta_{100} = (2D_a \tilde{q}_{b_{\mathrm{NET}}} \eta_0 \sigma^3 x)^{\frac{1}{2}}. \tag{5.14}$$

We can solve for the distance $x_s$ required for complete separation of small particles from large ones, i.e. when $\delta_0 = \delta_{100}$ (see figure 6). Equating (5.12) and (5.14) gives

$$x_s = \frac{h^2}{2D_a \tilde{q}_{b_{\mathrm{NET}}}(1+\eta_0 \sigma^3)}. \tag{5.15}$$

## 6. General solution

The above method-of-characteristics approach can also be applied to treat the more general cases when $\eta = n_b/n_a$ is not necessarily small but takes arbitrary values. Using (3.2), (3.17), (3.19), (3.20), (3.22), (3.23), (3.25), (3.27), (3.29), (3.30) in (3.24) and (3.26) we obtain the non-dimensional volume-averaged velocity of the small, $b$, and large, $a$, particles in the positive $y$-direction respectively:

$$\tilde{q}_b = \frac{-q_b}{D_a(\mathrm{d}u/\mathrm{d}y)}$$
$$= G(\eta, \sigma)\left[\bar{E} - E_{\mathrm{m}} + 1 + \frac{(1+\eta)\sigma}{(1+\eta\sigma)}\right] \exp\left[\frac{(1+\eta)\sigma/(1+\eta\sigma) - E_{\mathrm{m}}}{\bar{E} - E_{\mathrm{m}}}\right], \tag{6.1}$$

$$\tilde{q}_a = \frac{-q_a}{D_a(\mathrm{d}u/\mathrm{d}y)}$$
$$= G(\eta, \sigma)\left[\bar{E} - E_{\mathrm{m}} + 1 + \frac{(1+\eta)}{(1+\eta\sigma)}\right] \exp\left[-\frac{(1+\eta)/(1+\eta\sigma) - E_{\mathrm{m}}}{\bar{E} - E_{\mathrm{m}}}\right] \tag{6.2}$$

where $$G(\eta, \sigma) = \frac{4k_{\mathrm{LT}}^2 (M/N)(1+\eta\sigma)}{\pi(1+\eta)\{(1+\eta)[1+\eta\sigma^2]/(1+\eta\sigma)^2 + (\bar{E}^2)/(k_{\mathrm{AV}})(M/N)\}}.$$

From (3.25), (3.27), (3.28) and (4.4) we obtain the expressions for the non-dimensional net percolation velocities for the $b$ particles as

$$\tilde{q}_{b_{\mathrm{NET}}} = \frac{-q_{b_{\mathrm{NET}}}}{D_a(\mathrm{d}u/\mathrm{d}y)} = \frac{1}{(1+\eta\sigma^3)}(\tilde{q}_b - \tilde{q}_a), \tag{6.3}$$

and for $a$ particles as

$$\tilde{q}_{a_{\mathrm{NET}}} = \frac{-q_{a_{\mathrm{NET}}}}{D_a(\mathrm{d}u/\mathrm{d}y)} = -\frac{\eta\sigma^3}{(1+\eta\sigma^3)}(\tilde{q}_b - \tilde{q}_a). \tag{6.4}$$

The mass conservation equation (5.4) for $b$ particles can be rewritten as

$$u(y)\frac{\partial \rho_b}{\partial \eta}\frac{\partial \eta}{\partial x}+\frac{\partial}{\partial \eta}(\rho_b q_{b_{\mathrm{NET}}})\frac{\partial \eta}{\partial y}=0. \tag{6.5}$$

Assuming a linear velocity profile and substituting (5.5) into (6.5), we obtain the following equation, which is analogous to (5.6):

$$y\frac{\partial \eta}{\partial x}-D_a K_b\frac{\partial \eta}{\partial y}=0, \tag{6.6}$$

where

$$K_b=\gamma\frac{\partial}{\partial \eta}(-\rho_b q_{b_{\mathrm{NET}}})\Big/\left(\frac{\partial \rho_b}{\partial \eta}\right), \tag{6.7}$$

and $K_b$ can be obtained by simply differentiating (3.25) and (4.4$b$) with respect to $\eta$ and substituting into (6.7). The algebra is very lengthy and the full expression for $K_b$ is presented in Appendix A. From the method of characteristics, we find the solution of (6.6) to be

$$\eta=\frac{n_b}{n_a}=f\left(x+\frac{y^2}{2D_a K_b}\right). \tag{6.8}$$

This is similar in form to (5.7) which was obtained assuming a dilute concentration of fines, $\eta=n_b/n_a\to 0$.

We follow the same procedure to determine the complete separation of small particles from large ones as described in the previous section. The family of characteristic lines is given by

$$y=[y_0^2-2D_a K_b x]^{\frac{1}{2}}, \tag{6.9}$$

where $y_0$ is a constant corresponding to the $y$-value of the characteristic line at the initial station $x=0$. Consider a flow of uniform depth $h$ in which the initial concentration at $x=0$ is uniform over the depth such that

$$\eta(0, y)=\eta_0=\text{const.} \tag{6.10}$$

The 0% fines fall line $y=\delta_0(x)$ given by (6.9) becomes

$$\delta_0=[h^2-2D_a K_b x]^{\frac{1}{2}}. \tag{6.11}$$

The 100% fines accumulation line, $y=\delta_{100}(x)$, is obtained by using (5.13) for the depth-averaged conservation of mass, which yields

$$\delta_{100}=[2D_a K_b \eta_0 \sigma^3 x]^{\frac{1}{2}} \tag{6.12}$$

The distance for complete separation of small particles from large ones is found by equating (6.11) and (6.12), which gives

$$x_s=\frac{h^2}{2D_a K_b(1+\eta_0\sigma^3)}. \tag{6.13}$$

Substituting (6.13) into (6.11) we obtain the final depth of the fines layer after complete separation has occurred:

$$y_s=\left(\frac{\eta_0\sigma^3}{1+\eta_0\sigma^3}\right)^{\frac{1}{2}}h. \tag{6.14}$$

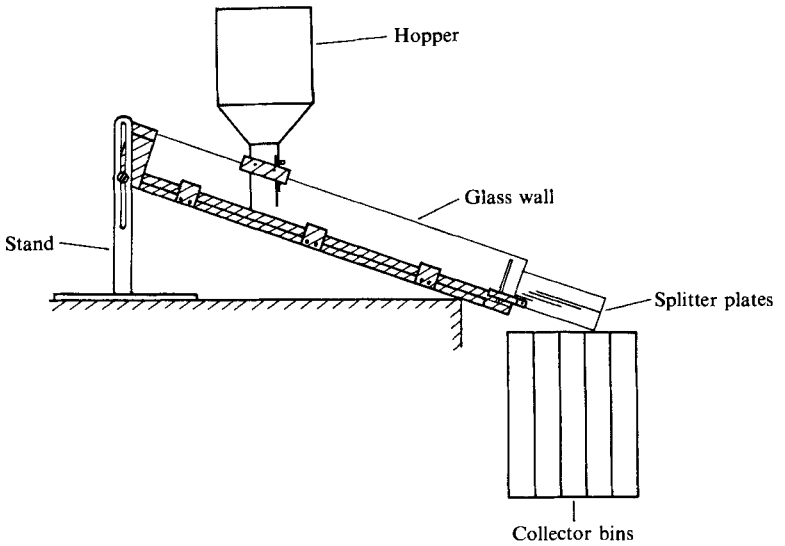


FIGURE 7. Schematic diagram of inclined-chute segregation apparatus.

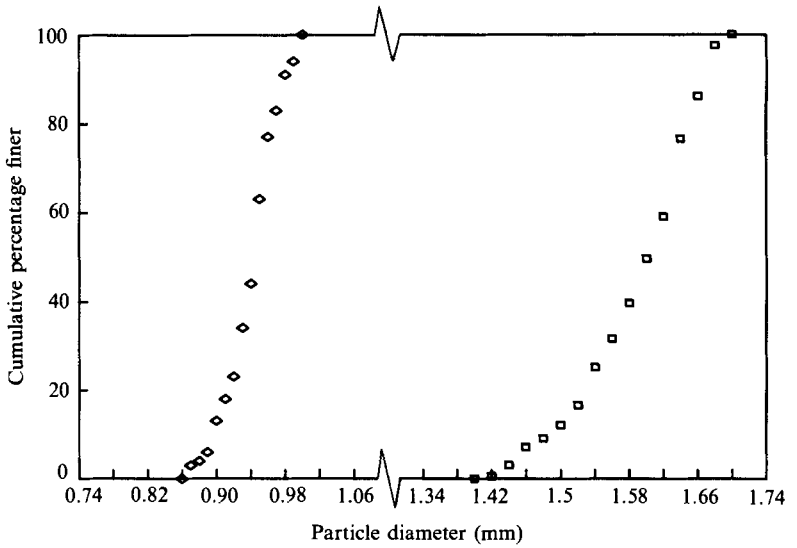


FIGURE 8. Size distributions ◇, 'small' spherical polystyrene beads; and □, 'large' spherical polystyrene beads.

## 7. Experimental measurements

Experiments were performed using the apparatus shown in figure 7. A Plexiglas hopper contained randomly mixed spherical polystyrene beads having a specific gravity of 1.095. The binary mixture was made up of large beads ranging from 1.40 to 1.68 mm in diameter and small 0.85 to 1.0 mm beads, having mean particle diameters of 1.6 and 0.943 mm respectively, giving a diameter ratio of 0.589. The size distributions for the small and large particles are shown in figure 8. These were determined by measuring the diameters of samples of several hundred particles with a micrometer. The mean angle of repose for the 'monosized' beads is 25°. No

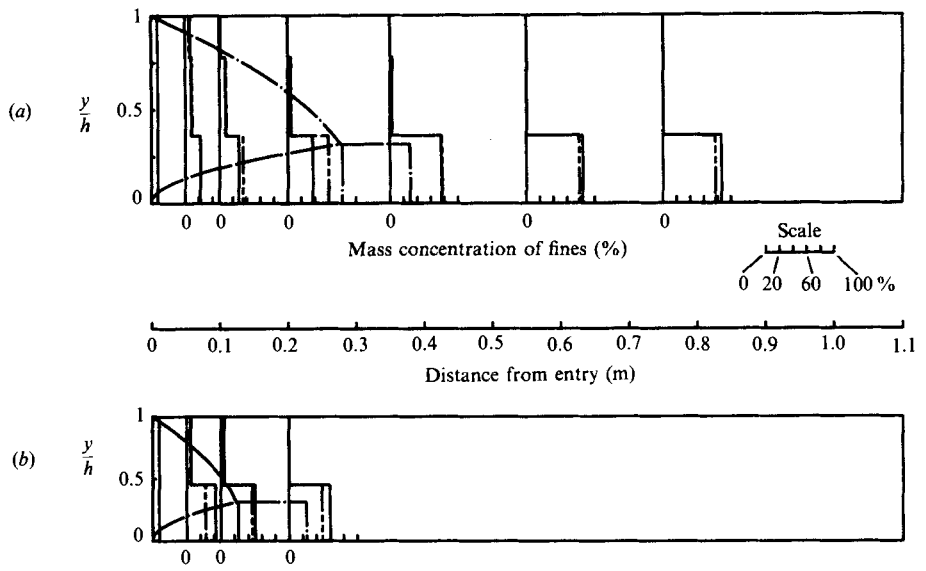


FIGURE 9. Concentration profiles for small particles (dilute theory); 10% initial concentration, chute inclination of 26°: (*a*) initial depth of entry, $h_0 = 15$ mm; (*b*) 10 mm. Concentration profiles averaged over gap between splitter plates: ——, measured concentration profile; — - —, predicted concentration profile; — · —, 0% fines fall line and 100% fines accumulation line and *unadjusted* concentration profile.

significant difference of mean angle of repose was found between the 'monosized' beads and the mixtures of 10% and 15% volume concentration of fines.

The hopper could be attached at any position along the inclined chute. The chute was 1 m in total length and the width of the channel cross-section was 75 mm; it had smooth glass sidewalls and a rough bottom. The particles flowed down the inclined chute and struck a series of splitter plates which were fixed to the downstream end of the chute and arranged to separate the flow into a maximum of five distinct layers. The layers of particles were then directed towards and collected in separate bins. By measuring the concentration of fines in each bin, the concentration profiles can be obtained at a given distance downstream from the hopper exit. By fixing the hopper at various positions along the chute, the development of the segregation process with distance along the chute can be determined. The chute can be tilted to provide different angles of inclination.

The flow depth of the mixture was observed to vary slightly along the streamwise direction; the amount of variation depended upon the flow rate and bed inclination angle. Thus, at the location where the flow struck the splitter plates, the flow depth was slightly different from the initial depth and not exactly equal to it, as assumed in the theory. Figures 9–13 show concentration profiles at different streamwise positions. The results are presented in terms of a non-dimensional coordinate formed by the ratio of the normal distance from the bed to the local depth of flow.

The values of $\bar{E}$, $M/N$ and $k_{AV}$ used in all the calculations were 0.701, 0.6 and 0.712 respectively. These values correspond to the case of five equal-sized particles around a void in a layer (see table 1) and they are felt to be reasonable values for the present inclined-chute experiments. Using (3.32) the values of bulk solids fraction $\nu$ are found to be 0.518 and 0.531 for the cases of 10% and 15% fines respectively. These values of $\nu$ are slightly lower than the value of $\nu = 0.546$ that gives a reasonably good fit to

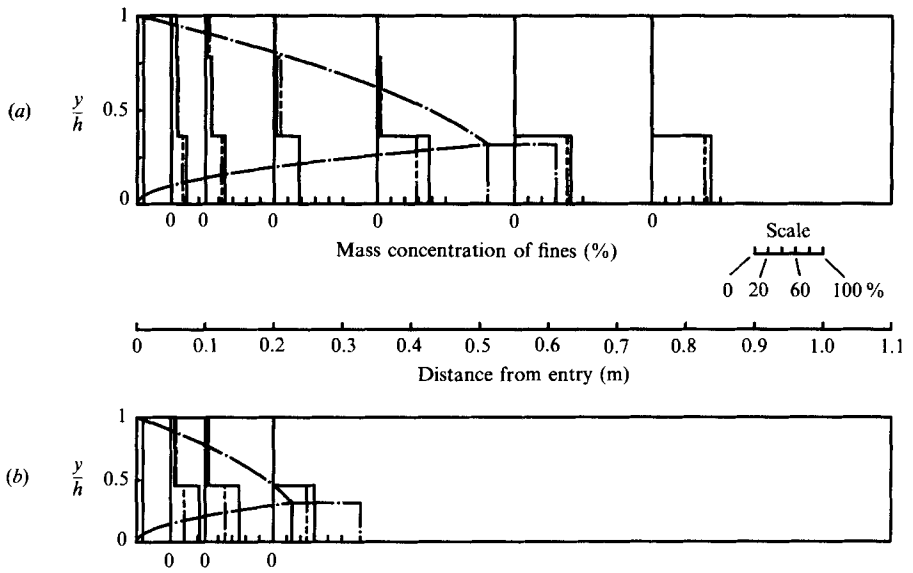


FIGURE 10. Concentration profiles for small particles (general theory); 10% initial concentration, chute inclination of 26°: (*a*) initial depth of entry, $h_0 = 15$ *mm*; (*b*) 10 mm. Curves designated as in figure 9.

the experimental data of Cooke & Bridgwater (1979) shown in figure 4 for $\sigma = 0.589$. It seems plausible that for continued shearing $\nu$ would be slightly smaller than for the reciprocal shearing of figure 4.

Figure 9 presents some typical experimental results for the case of a 10% initial concentration $C_{b0}$ at entry ($x = 0$) and an angle of inclination of 26°. As the flow proceeds downstream, the fines percolate towards the bottom. A layer consisting of 100% fines develops at the bed, its depth increases with downstream distance as indicated by the measured mass-concentration profile. (Note that the volume concentration of the small, $b$, particles $C_b$ given by (4.7) is the same as the mass concentration of small particles since the mass densities of the large and small particles are the same). By about 0.55 m from the entry, the fines have been separated from the coarse particles. This is not immediately obvious from figure 9, since the measured concentration of fines in the lowermost layer is only about 83%. The depth of the 100% fines layer was less than the height of the lowest splitter plate, hence both coarse and fines were collected to give an average measured concentration over the lowest gap of 83% at the separation distance $x_s$. It should also be noted that the splitter plates locally obstructed the flow, changing the velocity profiles and increasing the depth just in front of the splitter plate. Thus the measured concentration profiles shown in figure 9 are probably slightly different from what would exist in unobstructed flow. However, the distance required for complete separation of the fines should be very close to that obtained in the absence of the splitter plates. Figure 9 also shows the theoretical 0% fines fall line, the 100% fines accumulation line near the bed and the station for complete separation of fines based upon the asymptotic solution for dilute concentrations of fines using (5.12) and (5.14). The concentration profiles predicted by the present theory were obtained by averaging over depths corresponding to the gaps between individual splitter plates (for details see Appendix B). This was done to facilitate more direct comparison with the experimentally measured profiles.

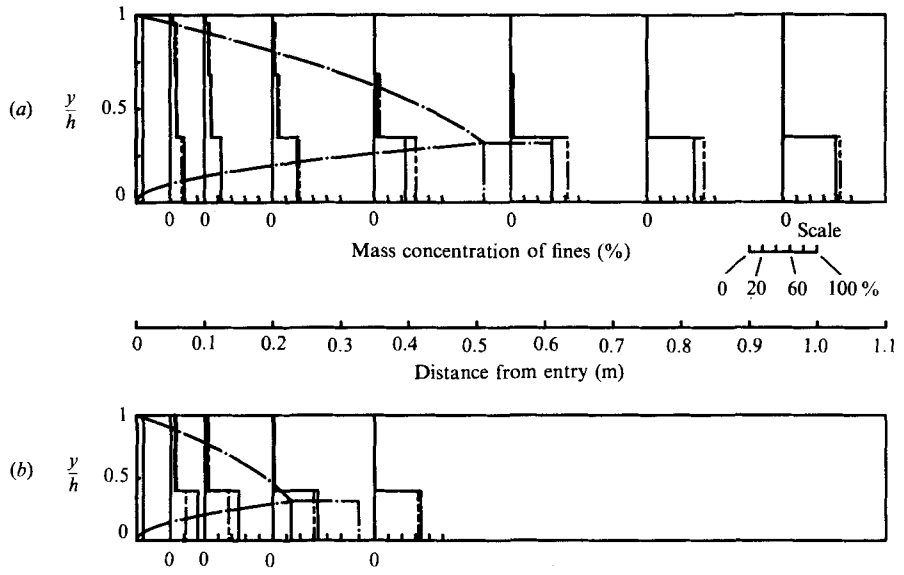


FIGURE 11. Concentration profiles for small particles (general theory); 10% initial concentration, chute inclination of 28°: (*a*) initial depth of entry, $h_0 = 15$ mm; (*b*) 10 mm. Curves designated as in figure 9.

The same set of experimental results is compared in figure 10 with the theoretical predictions based upon the *general* method-of-characteristics solution using (6.11) and (6.12). Comparing figures 9 and 10, the general theory is found to predict a length for complete separation of fines from coarse particles longer than that predicted by the asymptotic dilute theory.

Figure 11 presents similar comparisons of the present general theory with the experimental results for the case of 10% initial concentration of fines and 28° of inclination. Comparing figures 11 and 10, it is interesting to observe that the complete separation distance indicated by the measured concentration profiles increases with the angle of inclination. At higher angles of inclination the bulk material flows at a higher rate and the bulk solids fraction decreases (or correspondingly, the voids fraction increases). Hence, one would expect that the rate at which fines percolate down towards the bed will be larger since there are more voids that can accept the small particles. As a result, one might expect the complete separation distance to be shorter. However, the opposite trend is observed in the experimental results. The same is true for the experimental results for the case of 15% initial concentration of fines as presented in figures 12 and 13 for angles of inclination of 25° and 28° respectively.

The present general theory (which can handle arbitrary concentrations) offers a plausible explanation for the above behaviour. For example, consider the case of 10% initial concentration of fines. The non-dimensional volume-averaged velocities and the non-dimensional net percolation velocities for the small, $b$, and large, $a$, particles, which are given by (6.1)–(6.4), are plotted versus the bulk solids fraction in figure 14. To obtain values of the bulk solids fraction from (3.32), values of $\bar{E}$, $M/N$ and $k_{\mathrm{AV}}$ from table 1 together with interpolated values were used in the general theory. As shown in figure 14, the non-dimensional net percolation velocities of both the small particles, $\tilde{q}_{b_{\mathrm{NET}}}$, and large particles, $\tilde{q}_{a_{\mathrm{NET}}}$, increase to maximum values and

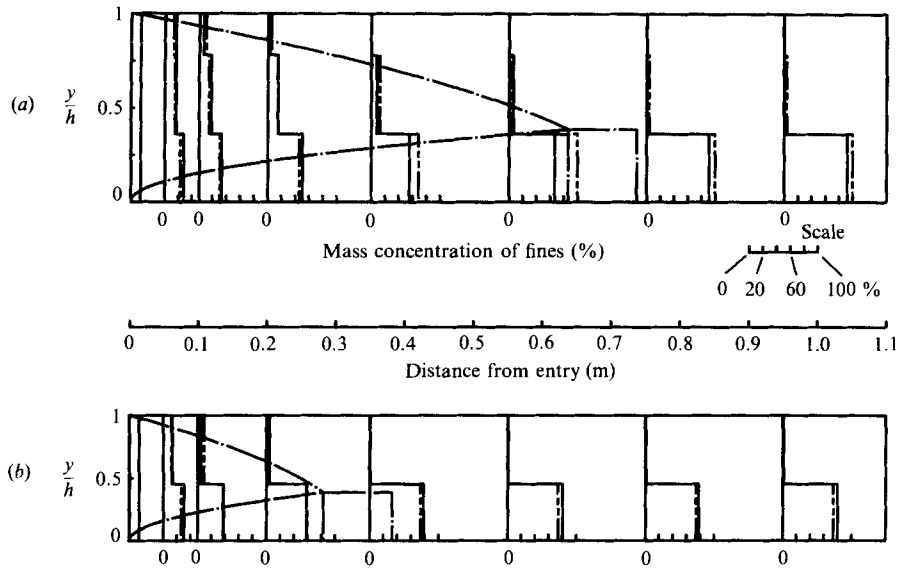


FIGURE 12. Concentration profiles for small particles (general theory); 15% initial concentration, chute inclination of 26°: (*a*) initial depth of entry, $h_0 = 15$ mm; (*b*) 10 mm. Curves designated as in figure 9.

then decrease as the bulk solids fraction decreases. When the bulk solids fraction is less than some critical value, the small particles percolate downward at a slower rate. The reason is that the voids become so large that a significant number of large particles find voids large enough for them to fall into, thus reducing the net percolation velocities of both the small and the large particles. This effect can be seen in the plots of the non-dimensional volume-averaged velocities of both the small particles, $\tilde{q}_b$, and large particles, $\tilde{q}_a$, as shown in figure 14. The rate at which $\tilde{q}_a$ increases with *decreasing* bulk solids fraction is higher than the rate of increase of $\tilde{q}_b$. As a result, it can take a longer distance for the complete separation of fines from coarse particles when the bulk solids fraction of the flowing materials decreases below some critical value.

The increase in separation distance with increased slope could also be due in part to effects that have been neglected in the present analysis. As the slope increases the velocities increase, the material becomes less dense and the magnitude of the individual particle velocity fluctuations increases. Under such conditions diffusive mixing of the particles becomes more important and segregation effects are thus inhibited.

Finally we make some comments about the use of the continuum approach for comparison with these experiments in which the thickness of the shearing layer is only several particle diameters thick. A related issue arises in comparisons of experimental shear flows with the kinetic theories of granular flow (see the review of Savage 1984). It is natural for one to immediately assume that to make the transition from a treatment at the level of individual particle interactions to the consideration of a continuum requires the shear layer to be many particle diameters thick. That this is not necessarily so can be seen from the analyses of transport properties in a granular shear flow (for example, see Lun *et al.* 1984) which are extensions of the kinetic theories of dense gases (Chapman & Cowling 1970). These analyses proceed to

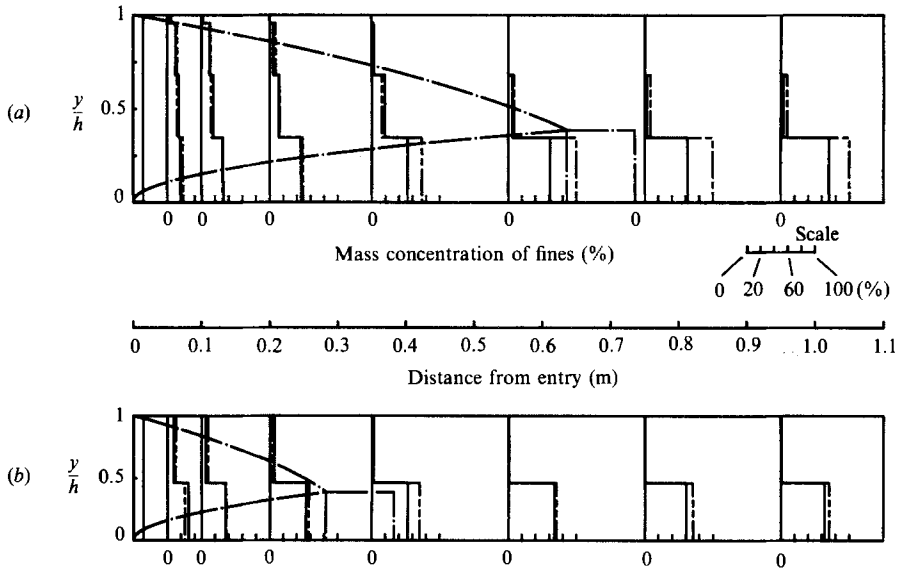


FIGURE 13. Concentration profiles for small particles (general theory); 15% initial concentration, chute inclination of 28°: (*a*) initial depth of entry, $h_0 = 15$ mm; (*b*) 10 mm. Curves designated as in figure 9.

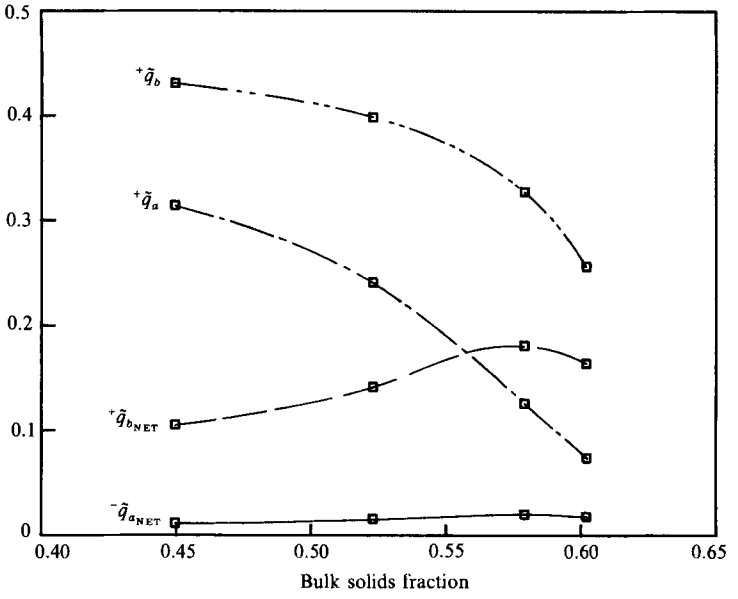


FIGURE 14. Predicted variation of non-dimensional net percolation velocities, $\tilde{q}_{a_{NET}}$ and $\tilde{q}_{b_{NET}}$, and non-dimensional volume-averaged velocities, $\tilde{q}_a$ and $\tilde{q}_b$ with bulk solids fraction for uniform initial concentration of 10% fines and $D_a/D_b = 0.589$.

determine stresses, energy fluxes, etc. by considering particle transport and collisions across an infinitely thin plane surface. The essential issue is to consider a sufficient number of particle interactions to make the statistical averages and the definition of the distribution functions meaningful. In the present paper we consider steady-state transport of particles across surfaces parallel to the bed of the inclined chute. This

means that we must consider a region of sufficient streamwise and lateral extent or a sufficiently long time for meaningful statistics, but it does not imply that the lengthscales perpendicular to the bed need to be many particle diameters in size.

## 8. Concluding remarks

The present paper has made use of information-entropy concepts to study the process of gravity separation of fine from coarse particles during the shearing flow of initially randomly mixed material down an inclined chute. The mechanism proposed to explain this process is essentially a kinematic one which involves the shearing of particles in relatively distinct layers and the tendency of particles in an upper layer to fall into randomly generated holes in the layer underneath.

The analyses have predicted the streamwise development of the particle concentration profiles, the development of the layer of 100% fine particles near the bed and the length for complete separation of fine from coarse particles. On the basis of the agreement between the predicted and experimentally observed behaviour it appears that the proposed flow mechanisms are reasonable, at least for the relatively slow flow regime.

To study the segregation process for the high-shear-rate flow regime one could apply kinetic theories for mixtures of granular materials of the kind recently developed by Farrell, Lun & Savage (1986). Such an approach would be applicable at moderate overall solids concentrations, and shear rates sufficiently high that the dominant contributions to the total stresses are due to interparticle collisions and that the effects of enduring frictional contacts are negligible. In the present experiments the flows occurred at relatively high bulk solids concentrations, at moderate shear rates and particles were observed to be in nearly constant contact with their neighbours. Under these conditions the present kinematic description of the segregation process would seem to be more appropriate than that which might be developed from the kinetic theory of mixtures of Farrell *et al.* (1986).

Grateful acknowledgement is made to the Natural Science and Engineering Research Council of Canada (NSERC) for the support of this work through an NSERC operating grant. The small $\eta$ theory appropriate for dilute concentrations of fine particles was presented by the senior author at the *1st European Symposium on the Stress and Strain Behaviour of Particulate Solids*, *8th International Congress of Chemical Engineering*, September 3–7, 1984, Prague, Czechoslovakia. The authors are greatly indebted to Janet Lees for formatting the equations and word processing. Acknowledgement is also made to the referees for numerous useful suggestions and comments.

## Appendix A. Summary of equations used in the general theory

From (3.25) and (4.4*b*), equation (6.7) for $K_b$ can be expressed as follows:

$$K_b(\eta) = \frac{4}{\pi}\frac{M}{N}\gamma k_{\mathrm{LT}}^2 \frac{\partial \mathrm{II}}{\partial \eta}\Big/\frac{\partial \mathrm{I}}{\partial \eta}, \tag{A 1}$$

where

$$\mathrm{I} = A_7/A_6, \tag{A 2}$$

$$\mathrm{II} = [A_2 \exp(A_3) - A_4 \exp(A_5)]/A_1 A_6^2 \tag{A 3}$$

and

$$A_1 = \frac{(1+\eta\sigma)^2(1+\eta\sigma^3)}{(1+\eta)\eta}, \tag{A 4}$$

$$A_2 = \bar{E} - E_m + 1 + \frac{(1+\eta)\sigma}{1+\eta\sigma}, \tag{A 5}$$

$$A_3 = -\frac{[(1+\eta)\sigma/(1+\eta\sigma)] - E_m}{\bar{E} - E_m}, \tag{A 6}$$

$$A_4 = \bar{E} - E_m + 1 + \frac{1+\eta}{1+\eta\sigma}, \tag{A 7}$$

$$A_5 = -\frac{[(1+\eta)/(1+\eta\sigma)] - E_m}{\bar{E} - E_m}, \tag{A 8}$$

$$A_6 = \frac{(1+\eta)(1+\eta\sigma^2)}{(1+\eta\sigma)^2} + \frac{\bar{E}}{k_{AV}}\frac{M}{N}, \tag{A 9}$$

$$A_7 = \frac{(1+\eta)^2\eta}{(1+\eta\sigma)^3}. \tag{A 10}$$

## Appendix B. Concentration profile averaged over the splitter-plate gap

Consider the flow of a binary mixture having an initial concentration of fines $B_{b0}$ which is constant over the depth at station $x = 0$. The 0% fines fall line, $\delta_0$, defines the region under which the concentration of fines is $C_{b0}$ and above which it is zero (see figure 6). The 100% accumulation line, $\delta_{100}$, defines the region under which there are no coarse particles but only fines.

The method of measuring the concentration profiles used in the present experiment was to divide the flow into a number of distinct layers by means of a series of splitter plates. These plates were positioned at different levels parallel to the bed and had their leading edges located close to the same streamwise station near the downstream end of the chute. If the splitter plates are sufficiently close to the upstream entry of flow, $\delta_0$ and $\delta_{100}$ will intersect the splitter plates before they can intersect each other (i.e. the location of the end of the channel is less than the complete separation distance $x_s$). In order to facilitate comparison of the present theories with the experimentally determined concentration profiles, the following layer depth-averaging procedure was used. First consider the possible case in which $\delta_0$ intersects an arbitrary $i$th layer ($i = 1, 2, \ldots$) located between $y_i$ and $y_{i+1}$ ($i = 1$ represents the lowest layer and $y_1 = 0$ corresponds to the bed). The depth-averaged concentration for each layer can be obtained from the conservation-of-mass equation for the fine, $b$, particles which can be expressed as

$$\int_{y_i}^{y_{i+1}} \rho_b u \, dy = \int_{y_i}^{\delta_0} \rho_b u \, dy + \int_{\delta_0}^{y_{i+1}} \rho_b u \, dy. \tag{B 1}$$

We can rewrite (B 1) by using (37),

$$\int_{y_i}^{y_{i+1}} C_b u \, dy = \int_{y_i}^{\delta_0} C_{b0} u \, dy + \int_{\delta_0}^{y_{i+1}} C_b u \, dy. \tag{B 2}$$

Since the concentration of fines is zero above $\delta_0$, the second term on the right-hand side of (B 2) drops out. As a result, using (3.25) and (5.5) in (B 2) we obtain the layer depth-averaged concentration for the $i$th layer:

$$\bar{C}_b = \frac{(\delta_0^2 - y_i^2) C_{b0}}{y_{i+1}^2 - y_i^2}. \tag{B 3}$$

Similarly, for a second possible case in which $\delta_{100}$ intersects the $i$th layer we have

$$\int_{y_i}^{y_{i+1}} C_b u \, dy = \int_{y_i}^{\delta_{100}} C_b u \, dy + \int_{\delta_{100}}^{y_{i+1}} C_{b0} u \, dy. \tag{B 4}$$

The concentrations of fines are 100% below $\delta_{100}$ and $C_{b0}$ above $\delta_{100}$. Hence, we find that the concentration averaged over the depth is

$$\bar{C}_b = \frac{(\delta_{100}^2 - y_i^2) + (y_{i+1}^2 - \delta_{100}^2) C_{b0}}{y_{i+1}^2 - y_i^2}. \tag{B 5}$$

For the third possible case in which both $\delta_0$ and $\delta_{100}$ intersect the same $i$th layer, we have

$$\bar{C}_b = \frac{(\delta_{100}^2 - y_i^2) + (\delta_0^2 - \delta_{100}^2) C_{b0}}{y_{i+1}^2 - y_i^2}. \tag{B 6}$$

## REFERENCES


Bagnold, R. A. 1954 Experiments on a gravity-free dispersion of large solids spheres in a Newtonian fluid under shear. *Proc. R. Soc. Lond.* A **225**, 49–63.

Bridgwater, J. 1971 Rate of spontaneous interparticle percolation. *Trans. Instn Chem. Engrs* **49**, 163–169.

Bridgwater, J. 1976 Fundamental powder mixing mechanisms. *Powder Technol.* **15**, 215–236.

Bridgwater, J., Cook, H. H. & Drahun, J. A. 1985*a* Strain induced percolation. In *Instn Chem. Engrs Symposium Series No. 69*, pp. 171–191.

Bridgwater, J., Cooke, M. H. & Scott, A. M. 1978 Inter-particle percolation: Equipment development and mean percolation velocities. *Trans. Instn Chem. Engrs.* **56**, 157–167.

Bridgwater, J., Foo, W. S. & Stephens, D. J. 1985*b* Particle mixing and segregation in failure zones – theory and experiment. *Powder Technol.* **41**, 147–158.

Brown, C. B. 1978 The use of maximum entropy in the characterization of granular media. In *Proc. US–Japan Seminar on Continuum Mechanical and Statistical Approaches in the Mechanics of Granular Materials* (ed. S. C. Cowin & M. Satake), pp. 98–108. Tokyo: Gakujutsu Bunken Fukyukai.

Campbell, A. P. & Bridgwater, J. 1973 The mixing of dry solids by percolation. *Trans. Instn Chem. Engrs* **51**, 72–74.

Chapman, S. & Cowling, T. G. 1970 *The Mathematical Theory of Non-uniform Gases*, 3rd edn. Cambridge University Press.

Cooke, M. H. & Bridgwater, J. 1979 Interparticle percolation: A statistical mechanical interpretation. *Ind. Engng Chem. Fundam.* **18**, 25–27.

Cooke, M. H., Bridgwater, J. & Scott, A. M. 1978 Interparticle percolation: lateral and axial diffusion coefficients. *Powder Technol.* **21**, 183–193.

Drahun, J. A. & Bridgwater, J. 1981 Free surface segregation. In *Instn Chem. Engrs Symposium Series No. 65*, pp. S4/Q/1–S4/q/14.

Drahun, J. A. & Bridgwater, J. 1983 The mechanism of free surface segregation. *Powder Technol.* **36**, 39–53.

Farrell, M., Lun, C. K. K. & Savage, S. B. 1986 A simple kinetic theory for granular flow of binary mixtures of smooth, inelastic, spherical particles. *Acta Mech.* **63**, 45–60.

Foo, W. S. & Bridgwater, J. 1983 Particle migration. *Powder Technol.* **36**, 271–273.

Jaynes, E. T. 1963 Information theory and statistical mechanics. *Statistical Physics III* (ed. K. W. Ford), pp. 181–218.

Johanson, J. R. 1978 Particle segregation and what to do about it. *Chem. Engng* **85**, 183–188.

Lun, C. K. K., Savage, S. B., Jeffrey, D. J. & Chepuniy, N. 1984 Kinetic theories for granular flow: inelastic particles in Couette flow and slightly inelastic particles in a general flow field. *J. Fluid Mech.* **140**, 223–256.

Masliyah, J. & Bridgwater, J. 1974 Particle percolation: a numerical study. *Trans. Instn Chem. Engrs* **52**, 31–42.

Middleton, G. V. 1970 Experimental studies related to problems of flysch sedimentation. In *Flysch Sedimentology in North America* (ed. J. Lajoie), pp. 253–272. Toronto: Business and Economics Science Ltd.

Middleton, G. V. & Hampton, M. A. 1976 Subaqueous sediment transport and deposition by sediment gravity flows. In *Marine Sediment Transport and Environmental Management* (ed. D. J. Stanley & D. J. P. Swift), pp. 197–218. Wiley.

Naylor, M. A. 1980 The origin of inverse grading in muddy debris flow deposits – A review. *J. Sedimentary Petr.* **50**, 1111–1116.

Sallenger, A. H. 1979 Inverse grading and hydraulic equivalence in grain-flow deposits. *J. Sedimentary Petr.* **49**, 553–562.

Savage, S. B. 1984 The mechanics of rapid granular flows. *Adv. Appl. Mech.* **24**, 289–366.

Scott, A. M. & Bridgwater, J. 1975 Interparticle percolation: a fundamental solids mixing mechanism. *Ind. Engng Chem. Fundam.* **14**, 22–27.

Walker, R. G. 1973 Mopping up the turbidite mess. In *Evolving Concepts in Sedimentology* (ed. R. N. Ginsberg), pp. 1–37. Johns Hopkins Press.

Walton, O. R. 1983 Particle dynamics calculations of shear flow. *Mechanics of Granular Materials: New Models & Constitutive Relations.* (ed. J. T. Jenkins & M. Satake), pp. 327–338. Amsterdam. Elsevier.

Williams, J. C. 1976 The segregation of particulate materials. A review. *Powder Technol.* **15**, 245–251.

Wills, B. A. 1979 *Mineral Processing Technology.* Pergamon.

Zallen, R. 1983 *The Physics of Amorphous Solids.* Wiley.